

Moving Weighted Least Squares implementation in MoFEM

Karol Lewandowski, Łukasz Kaczmarczyk, Ignatios Athanasiadis, Chris J. Pearce

School of Engineering

University of Glasgow

Key Words: *finite element method, bone remodelling, fracture, moving least squares approximation, heterogeneity, computed tomography*

1. Moving Weighted Least Squares (MWLS)

The Moving Weighted Least Squares (MWLS) method is used to construct interpolation functions on a set of points to approximate a given spatially varying discrete field (in this case the scalar density field), $v(\mathbf{X}_i)$, and is widely used for various meshless methods [2]. In computer graphics, it is useful to reconstruct a surface from a set of points [7] through downsampling or upsampling. Numerous studies have also attempted to utilise the method within the context of Element-Free Galerkin approach as trial and test functions [3, 10, 9].

In the context of configurational fracture mechanics [6], the nodal forces $\tilde{\mathbf{G}}^h$ are dependent on the gradient of elastic energy over change of density, $\mathbf{B}_\mathbf{x}^\top \rho$. Therefore, the approximation of a spatially smooth density field is important in order to evaluate the configurational forces at the crack front. To approximate a given discrete field, $v(\mathbf{X}_i)$, with MWLS method at a node of the mesh in the material configuration, each node is considered separately and denoted here as a Target Point of Approximation (TPA). The coordinates of each TPA are denoted with vector \mathbf{X}_t and the approximated field at that location is evaluated as:

$$v^h(\mathbf{X}_t) = \sum_{\alpha=1}^q p_\alpha(\mathbf{X}_t) a_\alpha(\mathbf{X}_t) = \mathbf{p}^\top(\mathbf{X}_t) \mathbf{a}(\mathbf{X}_t) \quad (1.1)$$

where $v^h(\mathbf{X}_t)$ is the approximated value, $\mathbf{p}(\mathbf{X}_t)$ is the vector of complete basis functions and $\mathbf{a}(\mathbf{X}_t)$ is the vector of unknowns. It should be noted that in MWLS method, $\mathbf{a}(\mathbf{X}_t)$ is spatially varying rather than being constant as used in conventional Least Squares method. Moreover, q is the number of approximation functions that are built from Pascal's tetrahedron via multiplicative combinations of unity with monomials equal to the spatial coordinates X_t , Y_t and Z_t of the TPA. For maximum target order of approximation functions, k , the total number of non-orthogonal approximation functions is determined by the binomial coefficient as:

$$q = \binom{k+3}{3} = \frac{(k+3)!}{6k!} \quad (1.2)$$

In the current implementation, three types of basis functions are used:

$$\begin{aligned} \mathbf{p}^\top(\mathbf{X}_t) &= \mathbf{p}^\top(X_t, Y_t, Z_t) = [1], & q = 1 \text{ and } k = 0, \\ \mathbf{p}^\top(\mathbf{X}_t) &= \mathbf{p}^\top(X_t, Y_t, Z_t) = [1, X_t, Y_t, Z_t], & q = 4 \text{ and } k = 1, \\ \mathbf{p}^\top(\mathbf{X}_t) &= \mathbf{p}^\top(X_t, Y_t, Z_t) = [1, X_t, Y_t, Z_t, X_t Y_t, Y_t Z_t, Z_t X_t, X_t^2, Y_t^2, Z_t^2], & q = 10 \text{ and } k = 2 \end{aligned} \quad (1.3)$$

For each TPA, the process to evaluate the vector of unknowns $\mathbf{a}(\mathbf{X}_t) = [a_1(\mathbf{X}_t), a_2(\mathbf{X}_t), \dots, a_q(\mathbf{X}_t)]$ in Eq. (1.1) involves consideration of neighbouring points of the discrete field $v(\mathbf{X}_i)$ and a weight function $w(r)$ is constructed, where r is the normalised radial distance from the TPA defined as $r = \|\mathbf{X}_t - \mathbf{X}_i\|/d_{mi}$ so that $0 < r \leq 1$, where d_{mi} is a scaling parameter.

An example of an arbitrary weight function for a 2D domain is presented in Figure 1. Values of the given discrete field $v(\mathbf{X}_i)$ are presented with dots and the positions where $v(\mathbf{X}_i)$ is mapped (i.e. TPAs) are presented with circles. Furthermore, the TPA under consideration is located at the origin of a cylindrical local coordinate system with r and w axes. For the 2D case, the weight function is visually represented as a 3D surface (shaded area) resulting from full rotation around w axis of the 1D weight function, $w(r)$, represented as a solid line. The boundary of the domain of influence of $w(r)$ is represented by a dashed circle ($r = 1$). $w(r)$ is equal to zero outside the domain of influence.

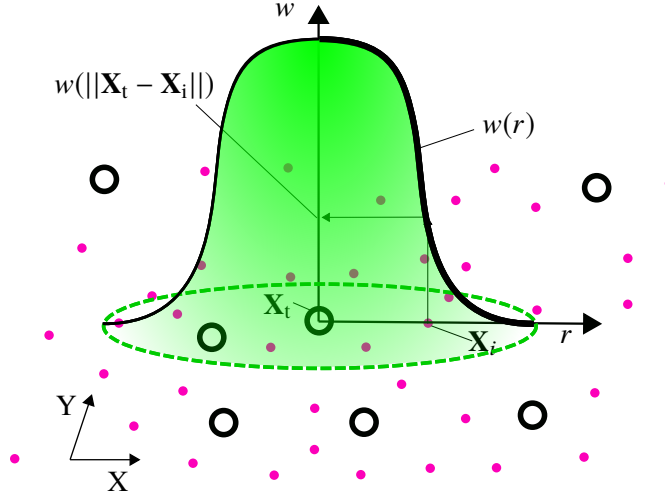


Figure 1: 2D schematic example of arbitrary weight function of a TPA located with position vector \mathbf{X}_t . Points of the discrete field $v(\mathbf{X}_i)$ are presented with dots and points that $v(\mathbf{X}_i)$ is mapped (TPAs) are presented with circles. The function is smooth, non-negative, reaches maximum at the TPA and decreases with distance $\|\mathbf{X}_t - \mathbf{X}_i\|$. The boundary of the domain of influence of the weight function is presented with dashed ellipsoid (circle on 2D plane) and the function takes a constant value of zero outside of it.

Many types of weight functions can be used for MWLS method. A one-dimensional quartic spline, commonly used in meshless methods [2], was chosen for the current work:

$$w(\|\mathbf{X}_t - \mathbf{X}_i\|/d_{mi}) = w(r_i) = \begin{cases} 1 - 6r_i^2 + 8r_i^3 - 3r_i^4 & \text{for } r_i \leq 1 \\ 0 & \text{for } r_i > 0 \end{cases} \quad (1.4)$$

Its derivative (required later) with respect to the material coordinates is:

$$\frac{dw}{d\mathbf{X}_t} = \frac{dw}{dr_i} \frac{dr_i}{d\mathbf{X}_t} = \frac{1}{d_{mi}} \begin{cases} (-12r_i + 24r_i^2 - 12r_i^3) & \text{for } r_i \leq 1, \\ 0 & \text{for } r_i > 0 \end{cases} \quad (1.5)$$

Here $r_i = \|\mathbf{X}_t - \mathbf{X}_i\|/d_{mi}$ is the normalised radial distance of point i from the TPA divided by scaling parameter d_{mi} . This coefficient is governing the size of influence domain.

With the above tools at hand, the vector of unknowns $\mathbf{a}(\mathbf{X}_t)$ associated to the TPA can be evaluated through minimisation of the weighted discrete L_2 norm:

$$J(\mathbf{X}_t) = \frac{1}{2} \sum_i^{n_w} w(r_i) \left(v^h(\mathbf{X}_t) - v(\mathbf{X}_i) \right)^2 = \frac{1}{2} \sum_i^{n_w} w(r_i) \left(\mathbf{p}^T(\mathbf{X}_i) \mathbf{a}(\mathbf{X}_t) - v(\mathbf{X}_i) \right)^2 \quad (1.6)$$

where $v(\mathbf{X}_i)$ is the value of the given discrete field at point i amongst the n_w points located within domain of influence of the TPA and $\mathbf{p}^T(\mathbf{X}_i)$ is the vector of shape functions of point i .

Minimisation of J with respect to \mathbf{a} leads to a system of linear equations as:

$$\mathbf{A}(\mathbf{X}_t) \mathbf{a}(\mathbf{X}_t) = \mathbf{B}(\mathbf{X}_t) \mathbf{v} \quad (1.7)$$

where matrices $\mathbf{A}(\mathbf{X}_t)$ and $\mathbf{B}(\mathbf{X}_t)$ are of size $(q \times q)$ and $(q \times n_w)$ and defined as follows:

$$\begin{aligned}\mathbf{A}(\mathbf{X}_t) &= \sum_i^{n_w} w(r_i) \mathbf{p}(\mathbf{X}_i) \mathbf{p}^T(\mathbf{X}_i) \\ \mathbf{B}(\mathbf{X}_t) &= \left[w(r_1) \mathbf{p}(\mathbf{X}_1), w(r_2) \mathbf{p}(\mathbf{X}_2), \dots, w(r_{n_w}) \mathbf{p}(\mathbf{X}_{n_w}) \right]\end{aligned}\quad (1.8)$$

and \mathbf{v} is $(n_w \times 1)$ vector of the given field values at the points within the influence domain given as:

$$\mathbf{v} = \left[v(\mathbf{X}_1), v(\mathbf{X}_2), \dots, v(\mathbf{X}_{n_w}) \right]^T \quad (1.9)$$

It should be noted that parameter d_{mi} is chosen to include sufficient n_w points such that the resulting matrix \mathbf{A} is not singular. Next, Eq. (1.1) combined with Eq. (1.7) can be rewritten as:

$$v^h(\mathbf{X}_t) = \sum_{i=1}^{n_w} \omega_i(\mathbf{X}_i) v_i = \boldsymbol{\omega}^T(\mathbf{X}_t) \mathbf{v} \quad (1.10)$$

where $\boldsymbol{\omega}(\mathbf{X}_t)$ is a resulting vector of shape functions associated with the TPA, defined as

$$\boldsymbol{\omega}^T(\mathbf{X}_t) = \mathbf{p}^T(\mathbf{X}_t) \mathbf{A}^{-1}(\mathbf{X}_t) \mathbf{B}(\mathbf{X}_t) \quad (1.11)$$

It is also necessary to approximate the density's gradient in the material domain. Therefore, the first derivative of the shape function with respect to the material coordinates is derived in direction X_j :

$$\boldsymbol{\omega}_{,j}^T = \mathbf{p}_{,j}^T \mathbf{A}^{-1} \mathbf{B} + \mathbf{p}^T (\mathbf{A}_{,j}^{-1} \mathbf{B} + \mathbf{A}^{-1} \mathbf{B}_{,j}) \quad (1.12)$$

The commas in the subscripts denote the partial derivative and the inverse of the material derivative of matrix \mathbf{A} is evaluated as

$$\mathbf{A}_{,j}^{-1} = -\mathbf{A}^{-1} \mathbf{A}_{,j} \mathbf{A}^{-1} \quad (1.13)$$

It is worth noting that for any TPA located at \mathbf{X}_β , MWLS shape functions do not satisfy Kronecker delta property, i.e. $\omega_i(\mathbf{X}_\beta) \neq \delta_{i\beta}$.

A common problem arising from CT scanning is generation of Partial Volume Artifacts [1]. As a result, the voxel data can be averaged between two materials, for example bone and soft tissue. To eliminate mapping spurious bone densities, some researchers have proposed to either redefine data at any node on the mesh surface to data assigned on the nearest internal node [5, 4] or resurface the mesh geometry [8]. In this study, a more elegant solution is proposed; every CT scan data point positioned outside the geometry of the bone is simply removed from the domain of influence, thereby only points that fall inside the volume are approximated. This procedure only has to be performed once for each domain of influence and can be easily parallelized.

2. MWLS mapping examples

Here, validation of the implementation of the MWLS method (described in 1) is presented via two examples. The first example involves the mapping of an analytical scalar field onto the nodes of a mesh of a prism. For this case, the relative error between the analytical input scalar field and MWLS results are compared for three target orders of approximation of MWLS. In the second example, mapping of CT scan data of a bone onto a mesh is presented. For this challenging mesh geometry, results of the MWLS method are compared with the direct CT scan data as well as results of least squares method.

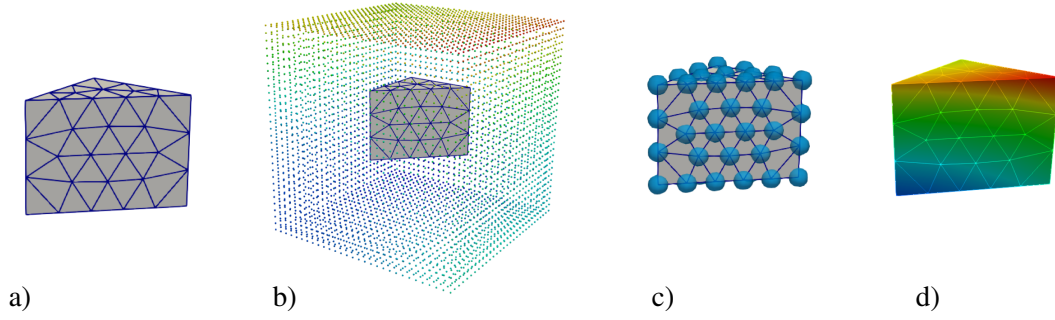


Figure 2: a) Finite element tetrahedral mesh. b) Mesh inside analytical discrete field $f(\mathbf{x}) = x + y^2 + z^3$. c) Mesh with corresponding nodes and spherical domain of influence. d) Results of the approximation for $q = 10$ projected onto mesh nodes.

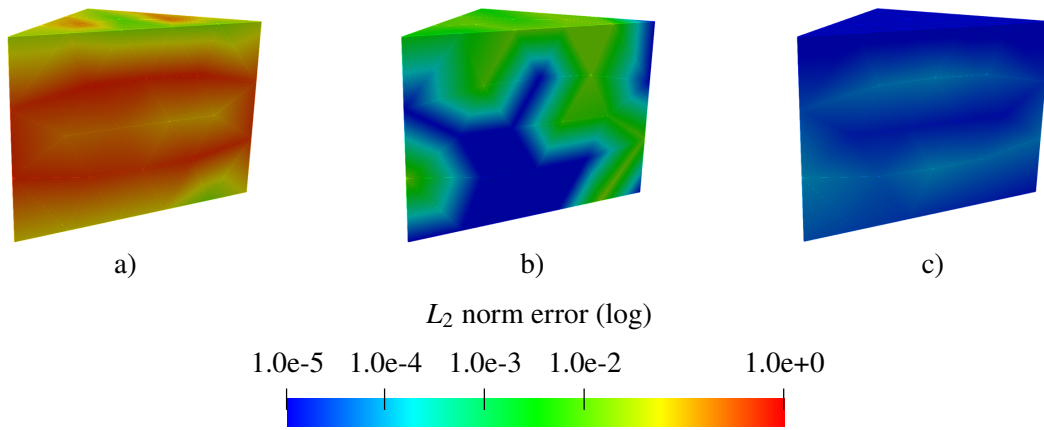


Figure 3: Contour plot of relative error of approximated gradient field for constant a), linear b) and quadratic c) basis functions. The logarithmic scale represents the magnitude of relative error.

2.1. Mapping of an analytical field

The analytical field ($f(\mathbf{x}) = x + y^2 + z^3$) is mapped onto the mesh nodes of the prism (Figure 2a) using the proposed MWLS procedure described in 1. The analytical field $f(\mathbf{x})$ is evaluated at a discrete set of points, $v(\mathbf{x}_i)$, presented in Figure 2b. The FE mesh is placed within the discrete field (Figure 2b) and the spherical domains of influence of each mesh node are presented (reduced in size for clearer visual presentation) in Figure 2c. The size of the influence domain is determined by increasing its radius until matrix \mathbf{A} in Eq. (1.7) is invertible for all mesh nodes. The approximated field data, with its gradient, is saved on corresponding nodes as demonstrated in Figure 2c for $q = 10$. Subsequently, the relative approximation error between the norm of analytical gradient of the given field $f(\mathbf{x})$ at the coordinates of each mesh node and the norm of gradient calculated with MWLS at the same node is evaluated and presented in Figure 3. The error is evaluated for three cases: constant ($q = 1$), linear ($q = 4$) and quadratic ($q = 10$) basis functions. It is clear from presented results in Figure 3 that constant functions are not sufficient for evaluating the gradient. The maximum error for a linear and quadratic basis has values of 10^{-2} and 10^{-4} , respectively. These results are satisfactory for the application of mapping data fields onto the mesh and suggest correctness of the implementation.

2.1.1. Metacarpal bone

In this section, the results of density approximation from CT data are presented. Geometry and finite element mesh of an equine 3rd metacarpal bone was obtained in ScanIP (Synopsys Simpleware, Exeter) from medical 3D images. The CT data was subsequently used to approximate the density values onto the

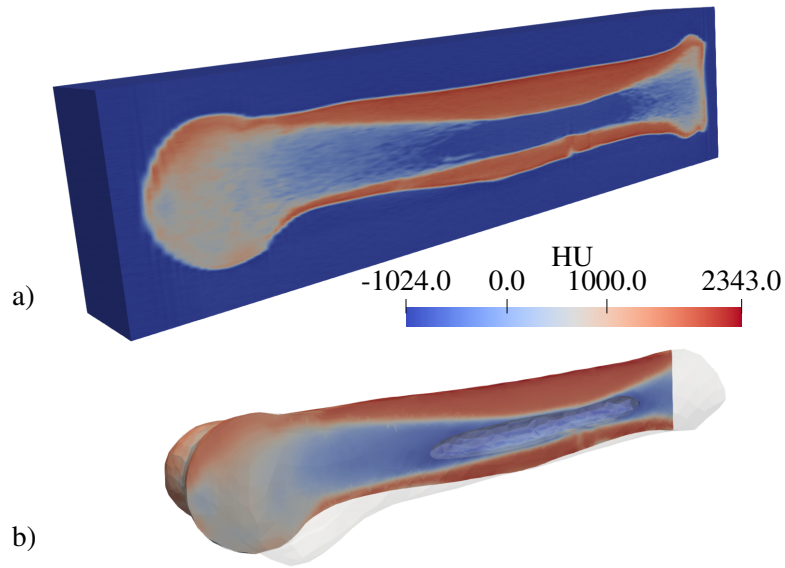


Figure 4: Comparison of a CT data with the corresponding approximation. a) A cut-view along the $x - y$ plane for CT scan data and b) density mapped onto FE mesh.

finite element mesh nodes by using the proposed MWLS method. The mesh consisted of approximately 7000 tetrahedral elements. Results of the mapping procedures are presented in Figure 4. Comparison between the proposed MWLS method and the standard Least Squares (LS) is shown in Figure 5 for both the density field and the density gradient field. The density pattern from both methods is very

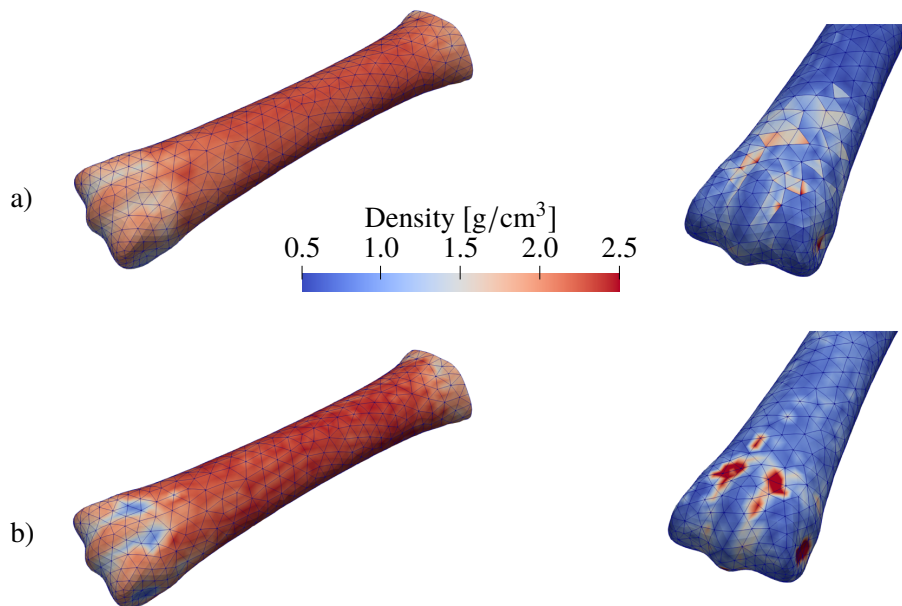


Figure 5: Mapping results of bone density (left) and density gradient (right). a) Least squares approximation. b) Moving Weighted Least Squares approximation.

similar. The MWLS method ensures that the density field is continuous despite the fact that the mesh is relatively coarse. This is particularly beneficial when using hierarchical basis functions, where larger elements with high order approximation can be more desirable. Classical finite elements provides only C^0 -continuity resulting in piecewise continuous gradients with LS. Density gradients resulting the MWLS approximation are smooth, as required for the fracture propagation analysis. It can also be seen that mesh boundary does not suffer from Partial Volume Artifacts [1].

3. Summary

This contribution investigated the application of a meshless MWLS method in approximating the density data on FE models. Validation of analytical field mapped on a simple mesh and comparison with LS method on mapping data from CT scanning was conducted and proved that MWLS can be a suitable technique for the approximation of density field, even with strong gradients. Nevertheless, the accuracy of the presented approach still has to be validated experimentally, for example, in the prediction of strains in the loaded bone specimen.

References

- [1] J. E. Adams. Quantitative computed tomography. *European journal of radiology*, 71(3):415–424, 2009.
- [2] T. Belytschko, Y. Krongauz, D. Organ, M. Fleming, and P. Krysl. Meshless methods: an overview and recent developments. *Computer methods in applied mechanics and engineering*, 139(1-4):3–47, 1996.
- [3] T. Belytschko and M. Tabbara. Dynamic fracture using element-free galerkin methods. *International Journal for Numerical Methods in Engineering*, 39(6):923–938, 1996.
- [4] G. Chen, B. Schmutz, D. Epari, K. Rathnayaka, S. Ibrahim, M. Schuetz, and M. Pearcy. A new approach for assigning bone material properties from ct images into finite element models. *Journal of biomechanics*, 43(5):1011–1015, 2010.
- [5] B. Helgason, F. Taddei, H. Pálsson, E. Schileo, L. Cristofolini, M. Viceconti, and S. Brynjólfsson. A modified method for assigning material properties to fe models of bones. *Medical engineering & physics*, 30(4):444–453, 2008.
- [6] Ł. Kaczmarczyk, Z. Ullah, and C. J. Pearce. Energy consistent framework for continuously evolving 3d crack propagation. *Computer Methods in Applied Mechanics and Engineering*, 324:54–73, 2017.
- [7] P. Lancaster and K. Salkauskas. Surfaces generated by moving least squares methods. *Mathematics of computation*, 37(155):141–158, 1981.
- [8] E. Peleg, R. Herblum, M. Beek, L. Joskowicz, M. Liebergall, R. Mosheiff, and C. Whyne. Can a partial volume edge effect reduction algorithm improve the repeatability of subject-specific finite element models of femurs obtained from ct data? *Computer methods in biomechanics and biomedical engineering*, 17(3):204–209, 2014.
- [9] Z. Ullah and C. Augarde. Finite deformation elasto-plastic modelling using an adaptive meshless method. *Computers & Structures*, 118:39–52, 2013.
- [10] K. C. Wong, L. Wang, H. Zhang, H. Liu, and P. Shi. Meshfree implementation of individualized active cardiac dynamics. *Computerized Medical Imaging and Graphics*, 34(1):91–103, 2010.